

# Corrugated metal-coated tapered tip for scanning near-field optical microscope

Tomasz J. Antosiewicz\*, Tomasz Szoplik

Faculty of Physics, Warsaw University, Pasteura 7, 02-093 Warszawa, Poland

\*Corresponding author: [tantos@igf.fuw.edu.pl](mailto:tantos@igf.fuw.edu.pl)

**Abstract:** This paper addresses an important issue of light throughput of a metal-coated tapered tip for scanning near-field microscope (SNOM). Corrugations of the interface between the fiber core and metal coating in the form of parallel grooves of different profiles etched in the core considerably increase the energy throughput. In 2D FDTD simulations in the Cartesian coordinates we calculate near-field light emitted from such tips. For a certain wavelength range total intensity of forward emission from the corrugated tip is 10 times stronger than that from a classical tapered tip. When realized in practice the idea of corrugated tip may lead up to twice better resolution of SNOM.

©2007 Optical Society of America

**OCIS codes:** (180.0180) Microscopy; (180.5810) Scanning microscopy; (240.5420) Polaritons; (240.6680) Surface plasmons; (240.6690) Surface waves; (350.4600) Optical engineering.

---

## References and Links

1. H. A. Bethe, "Theory of diffraction by small holes," *Phys. Rev.* **66**, 163–182 (1944).
2. E. H. Syngé, "A suggested method for extending the microscopic resolution into the ultramicroscopic region," *Phil. Mag.* **6**, 356 (1928).
3. E. A. Ash and G. Nichols, "Super-resolution aperture scanning microscope," *Nature* **237**, 510–512 (1972).
4. D. W. Pohl, W. Denk, and M. Lanz, "Optical stethoscopy: Image recording with resolution  $\lambda/20$ ," *Appl. Phys. Lett.* **44**, 651–653 (1984).
5. U. Dürig, D. W. Pohl, and F. Rohner, "Near-field optical-scanning microscopy," *J. Appl. Phys.* **59**, 3318–3327 (1986).
6. L. Novotny, D. Pohl, and B. Hecht, "Scanning near-field optical imaging using metal tips illuminated by higher-order Hermite-Gaussian beams," *Opt. Lett.* **20**, 970–972 (1995).
7. J. H. Kim and K. B. Song, "Recent progress of nano-technology with NSOM," *Micron* **38**, 409–426 (2007).
8. T. W. Ebbesen, H. J. Lezec, H. F. Ghaemi, T. Thio, and P. A. Wolff, "Extraordinary optical transmission through sub-wavelength hole arrays," *Nature* **391**, 667–669 (1998).
9. D. E. Grupp, H. J. Lezec, T. W. Ebbesen, K. M. Pellerin, and T. Thio, "Crucial role of metal surface in enhanced transmission through subwavelength apertures," *Appl. Phys. Lett.* **77**, 1569–1571 (2000).
10. H. J. Lezec, A. Degiron, E. Devaux, R. A. Linke, L. Martín-Moreno, F. J. García-Vidal, and T. W. Ebbesen, "Beaming light from a subwavelength aperture," *Science* **297**, 820 (2002).
11. F. J. García de Abajo, "Light transmission through a single cylindrical hole in a metallic film," *Opt. Express* **10**, 1475–1484 (2002) <http://www.opticsinfobase.org/abstract.cfm?URI=oe-10-25-1475>.
12. L. Martín-Moreno, F. J. García-Vidal, H. J. Lezec, A. Degiron, and T. W. Ebbesen, "Theory of highly directional emission from a single subwavelength aperture surrounded by surface corrugations," *Phys. Rev. Lett.* **90**, 167401 (2003).
13. F. I. Baida, D. Van Labeke, and B. Guizal, "Enhanced Confined Light Transmission by Single Subwavelength Apertures in Metallic Films," *Appl. Opt.* **42**, 6811–6815 (2003).
14. C. Genet and T. W. Ebbesen, "Light in tiny holes," *Nature* **445**, 39–46 (2007).
15. L. Novotny and C. Hafner, "Light propagation in a cylindrical waveguide with a complex, metallic, dielectric function," *Phys. Rev. E* **50**, 4094–4196 (1994).
16. S. Astilean, P. Lalanne, and M. Palamaru, "Light transmission through metallic channels much smaller than the wavelength," *Opt. Commun.* **175**, 265–273 (2000).
17. K. Y. Kim, Y. K. Cho, H. S. Tae, and J. H. Lee, "Optical guided dispersions and subwavelength transmissions in dispersive plasmonic circular holes," *Opto-Electron. Rev.* **14**, 233–241 (2006).
18. S. A. Maier and H. A. Atwater, "Plasmonics: Localization and guiding of electromagnetic energy in metal/dielectric structures," *J. Appl. Phys.* **98**, 011101-1-10 (2005).
19. A. V. Zayats, I. I. Smolyaninov, and A. A. Maradudin, "Nano-optics of surface plasmon polaritons," *Phys. Rep.* **408**, 131–314 (2005).

20. T. J. Antosiewicz and T. Szoplik, "Description of near- and far-field light emitted from a metal-coated tapered fiber tip," *Opt. Express* **15**, 7845-7852 (2007) <http://www.opticsinfobase.org/abstract.cfm?URI=oe-15-12-7845>.
21. E. X. Jin and X. Xu, "Obtaining super resolution light spot using surface plasmon assisted sharp ridge nanoaperture," *Appl. Phys. Lett.* **86**, 111106 (2005).
22. K. Tanaka, M. Tanaka, and T. Sugiyama, "Creation of strongly localized and strongly enhanced optical near-field on metallic probe-tip with surface plasmon polaritons," *Opt. Express* **14**, 832-846 (2006) <http://www.opticsinfobase.org/abstract.cfm?URI=oe-14-2-832>.
23. M. I. Stockman, "Nanofocusing of Optical Energy in Tapered Plasmonic Waveguides," *Phys. Rev. Lett.* **93**, 137404 (2004).
24. N. A. Janunts, K. S. Baghdasaryan, K. V. Nerkararyan, and B. Hecht, "Excitation and superfocusing of surface plasmon polaritons on a silver-coated optical fiber tip," *Opt. Commun.* **253**, 118-124 (2005).
25. W. Nakagawa, L. Vaccaro, and H.P. Herzig, "Analysis of mode coupling due to spherical defects in ideal fully metal-coated scanning near-field optical microscopy probes," *J. Opt. Soc. Am. A* **23**, 1096-1105 (2006) <http://www.opticsinfobase.org/abstract.cfm?URI=josaa-23-5-1096>.
26. Z. Ma, J.M. Gerton, L.A. Wade, and S.R. Quake, "Fluorescence Near-Field Microscopy of DNA at Sub-10 nm Resolution," *Phys. Rev. Lett.* **97**, 260801 (2006).
27. W. Ding, S.R. Andrews, and S.A. Maier, "Internal excitation and superfocusing of surface plasmon polaritons on a silver-coated optical fiber tip," *Phys. Rev. A* **75**, 063822 (2007).
28. S.T. Huntington, B.C. Gibson, J. Canning, K. Digweed-Lyytikäinen, J.D. Love, and V. Steblina, "A fractal-based fibre for ultra-high throughput optical probes," *Opt. Express* **15**, 2468-2475 (2007) <http://www.opticsinfobase.org/abstract.cfm?URI=oe-15-5-2468>.
29. C. Obermüller and K. Karrai, "Far field characterization of diffracting circular aperture," *Appl. Phys. Lett.* **67**, 3408-3410 (1995).
30. A. Gademann, I.V. Shvets, and C. Durkan, "Study of polarization-dependant energy coupling between near-field optical probe and mesoscopic metal structure," *J. Appl. Phys.* **95**, 3988-3993 (2004).
31. T. Szoplik, W. M. Saj, J. Pniewski, and T.J. Antosiewicz, "Transmission of radially polarized light beams through nanoholes," Abstracts of the EOS Topical Meeting on Nanophotonics, Metamaterials and Optical Microcavities, 16-19 October 2006, Paris, France.
32. A. Drezet, S. Huant, and J. C. Woehl, "In situ characterization of optical tips using single fluorescent nanobeads," *J. Lumin.* **107**, 176-181 (2004).
33. W. Saj, "FDTD simulations of 2D plasmon waveguide on silver nanorods in hexagonal lattice," *Opt. Express* **13**, 4818-4827 (2005) <http://www.opticsinfobase.org/abstract.cfm?URI=oe-13-13-4818>.
34. C. Sönnichsen, *Plasmons in metal nanostructures*, PhD Thesis (Ludwig-Maximilians-Universität München, München, 2001).
35. P. Johnson and R. Christy, "Optical Constants of the Noble Metals," *Phys. Rev. B* **6**, 4370-4379 (1972).
36. N. Fang, H. Lee, C. Sun, X. Zhang, "Sub-diffraction-limited optical imaging with a silver superlens," *Science* **308**, 534-537 (2005).

---

## 1. Introduction

Scanning near-field optical microscope (SNOM) with nowadays achievable resolution is good for watching sub-micron objects. When the distance between a sample and the tip aperture is kept constant, the resolution is limited by aperture diameter. An increase of the amount of light passing through the probe should allow for aperture diameter reduction. Therefore the most challenging issue is the improvement of light throughput of SNOM probes.

The research in near-field optical microscopy and near-field optics started with a paper on diffraction by small holes published by Bethe [1] in 1944. His work along with the idea of Synge [2] on the use of small apertures to image a surface with subwavelength resolution and the work of Ash and Nichols [3] led to the works of Pohl and co-workers [4, 5] on SNOM.

A SNOM aperture probe is a metal-coated tapered fiber tip that illuminates the surface of an analyzed sample through an uncoated orifice. The illuminated area of an object is a few times smaller than the wavelength. Present commercially available aperture SNOM probes usually do not reach resolutions better than 30 nm [6, 7]. The diameter size  $a$  of the aperture is critical for good resolution and should be as small as possible. However, the decrease of  $a$  drastically reduces the energy throughput. The amount of light scattered on the sample should match the detecting system's threshold value. To alleviate this problem one can increase the input energy. The downside of this is that the energy dissipated in the tapered part of the probe heats it up. As a result, the operating temperature of a typical SNOM tip may even exceed 400°C. Different thermal expansion coefficients of the core and metal cladding may

result in the flaking of the coating. The above mentioned issues prevent the usage of very small apertures and high energy inputs and thus limit the achievable resolution.

As a simple reduction of aperture diameter is not possible, an alternative solution should be sought. One way is to control the angle of divergence of light emitted in the near-field. Another is the increase of the transmission ability of SNOM probes. This could enable a reduction of the aperture size while keeping the output energy flux compatible with the sensitivity of detectors that collect the scattered light.

In the last years interest in nanooptical devices employing surface plasmon waves was connected with many important existing and potential applications. It was initiated by Ebbesen *et al.* [8] who observed transmission through arrays of subwavelength holes in a metal film increased with respect to Bethe's prediction. Later it was observed that single holes and slits in corrugated metal films also exhibit enhanced transmission [9-14]. This transmission increase results from excitation of surface plasmon-polaritons (SPPs) on the metal-dielectric interface. The coupling of surface waves to the periodic hole arrays and to periodic corrugations surrounding single holes makes it possible to tailor the transmission properties. Description of holes in terms of waveguide theory explains transmission of guided modes [15-17].

In this paper we employ the concept of enhanced transmission of subwavelength holes in corrugated metal films known in nanooptical plasmonic devices [14, 18, 19] and our recent model of SNOM probe radiation [20] to a novel shape of metal-coated tapered tips for SNOM. We propose that the interface between the fiber core and metal coating is structured into parallel grooves of different profiles curved inward the core. In 2D FDTD simulations we show that the corrugation increases total light transmission of a tip by a factor of 10 in comparison to the tip with smooth inner surface of the metal coating. The higher energy throughput is not accompanied by a widening of the beam and the angle of divergence is preserved. Two dimensional simulations in the Cartesian coordinates are chosen to use linearly polarized illumination.

## 2. Corrugated tip concept

Standard SNOM probes are characterized by low throughput which is on the order of  $10^{-4}$  for etched fibers and  $10^{-6}$  for pulled fibers. The reason for this low transmittance is the thinning of the tip below the cutoff diameter  $D = 0.6\lambda/n$ , where the propagation vector becomes imaginary and the wave decays exponentially [15, 7]. Large taper angles or non-circular apertures [21, 22] may improve the light throughput in aperture probes. Several other technical solutions in apertureless and photonic crystal fiber probes were reported to increase both energy throughput and resolution [23-28].

We propose another method for improving the efficiency of energy transport through SNOM probes that stems directly from our recently proposed model of charge density distribution on a metal-coated tapered tip [20]. For the first time, the model gives the far-field intensity distribution emitted by SNOM probe that is in agreement with experimental results [29]. Of course, the model valid in the far-field holds for the near-field. The crux of the model is that the charge is located solely on the rim of metal coating of the probe. This rim charge density distribution is described by cosine function with azimuthal dependence

$$\rho(r, \phi) \propto \cos(N\phi) \cos(\alpha r) \delta(r - R') \quad (1)$$

where  $N$  is the number of quasi-dipoles induced on the aperture circumference and  $R'$  is a hole radius. The desired improvement of energy throughput should result from an increase of charge density. In the final narrow segment of the tip, where the diameter is smaller than the cutoff  $D$ , there is only a standing evanescent wave, though the metallized tip with diameters below  $D$  still guides SPPs. This last mechanism should be enhanced to reach higher charge density at the probe end. Corrugation of the core-metal interface enhances the generation of propagating SPPs and localized plasmons in the fiber region from where the input beam cross-

section approaches the fiber diameter to the cutoff diameter and eases farther transport of the surface wave.

The grooves of different profiles oriented perpendicularly to the probe axis should not depolarize the propagating beam. Thus previously considered means to improve the SNOM resolution through polarization control remain valid [30, 31].

We are not aware of a thorough study that relates the Bethe's intensity dependence on the small hole aperture-to-wavelength ratio  $I \propto (a/\lambda)^4$  to radiation of SNOM probes with small diameters. We believe that in the case of SNOM metal-coated tips an exponential dependence may hold but the power is different from 4. Recently, Drezet *et al.* [32] mentioned difficulties with SNOM image interpretation that arise from this problem.

### 3. FDTD simulations: results and discussion

In simulations we use a fiber core of 2  $\mu\text{m}$  diameter tapered to 50 nm at the aperture. The taper angle is 20 degrees. This relatively small value is chosen to show how corrugations improve low transmittance connected with a small taper angle. We assume the probe is metallized with a 70 nm thick layer of silver. In Fig. 1(a) we present the end of the structure. This model probe is then modified with semicircular corrugations of 80 nm diameter curved inward the core and placed 370 nm apart with the first located 185 nm from the tip aperture as shown in Fig. 1(b). The second modification consists of rounded rectangular grooves 180 nm wide placed with a 370 nm period shown in Fig. 1(c). Their maximum depth and the radius of curvature are both 30 nm. The periodicity of corrugations is a trade-off between two opposite requirements. On one hand, we want a small period comparable with the plasmon wavelength. On the other, hand the bigger the period, the easier is the etching of the grooves. Consequently, the rectangular wide grooves should be easier to fabricate.

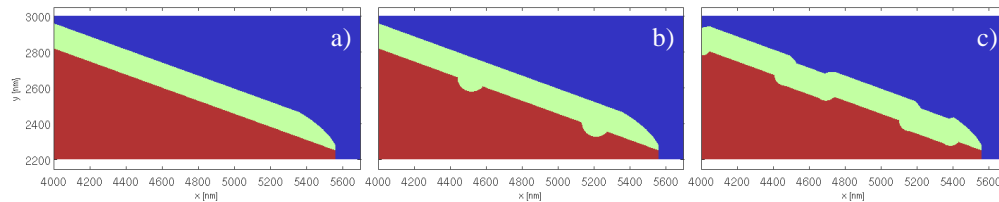


Fig. 1. Modeled tip structures without corrugations a), with semicircular b) and rounded rectangular c) corrugations. Colors indicate: glass core – dark red, metal coating – green, vacuum – blue. The pictures show, because of clarity, only the symmetrically cut, narrow end of the tips. The metal layer is chosen so that no simulated silver pixel is farther than 70 nm from the glass core. Structures will have the following labels: a) smooth tip, b) tip with semicircular grooves, c) tip with rounded rectangular grooves.

The structures are simulated using FDTD code EMFIDES of Saj [33] with an implementation of the Drude dispersion model

$$\varepsilon(\omega) = \varepsilon_{\infty} - \omega_p^2 [\omega(\omega + i\Gamma)]. \quad (2)$$

We use the following parameters:  $\varepsilon_{\infty} = 3.70$ ,  $\omega_p = 13673$  THz and  $\Gamma = 27.35$  THz calculated by Sönnichsen [34] from experimental data on reflection and transmission of silver films obtained by Johnson and Christy [35]. The glass core is modeled as dispersionless with refractive index  $n = 1.449$ . The wavelength range considered is 400–600 nm. As an excitation signal a CW Gaussian beam is used. Its width is chosen to minimize the field at the boundaries of the simulation. As a result the electric field's full-width at half-maximum (FWHM) is about one-third of the fiber core diameter of 2  $\mu\text{m}$  and the energy flow does not occupy the full area of the core.

In 2D FDTD simulations we analyze and compare beam profiles. To conform to our model [20] we use linearly polarized  $H_z$  illumination with the electric field in the plane of the simulation. The  $E_z$  polarization is not considered because it does not couple to SPPs. This

rules out the use of 2D FDTD in cylindrical coordinates. The 2D simulation is made in the Cartesian coordinates with space discretization 0.5 nm. Using our code EMFIDES a full 3D simulation would require about 6TB of RAM. Transmittance and FWHM of output beams in the near-field are the main parameters that show an advantage of corrugated SNOM probes over the classical tapered tip.

Figure 2 shows the calculated transmission spectra of three analyzed tips. The plots in Fig 2 (a) and (b) present absolute intensities and intensity spectra normalized to smooth tip transmission, respectively. Transmission is calculated as the ratio of the output energy integrated in a plane 10 nm outside the tip within 100 nm from the tip symmetry axis to the total input energy. The relatively high level of absolute light throughput in smooth tapered tip shown in Fig. 2(a) is possible when fiber core diameter is about 6 times bigger than the input Gaussian beam radius. If beams of broader profiles are used, the absolute transmission will be lower. The increase in transmission for small wavelengths is a result of tunneling through the metal coating. According to reflectance measurements the plasma frequency in silver corresponds to wavelength 311 nm. The tunneling for short wavelengths yields a signal almost as strong as the aperture radiation and that is the reason we do not observe a well defined beam. The most important information comes from the scaled intensity plot in Fig. 2(b). For different wavelength ranges we reach an almost tenfold increase in total transmitted energy for both corrugated tips.

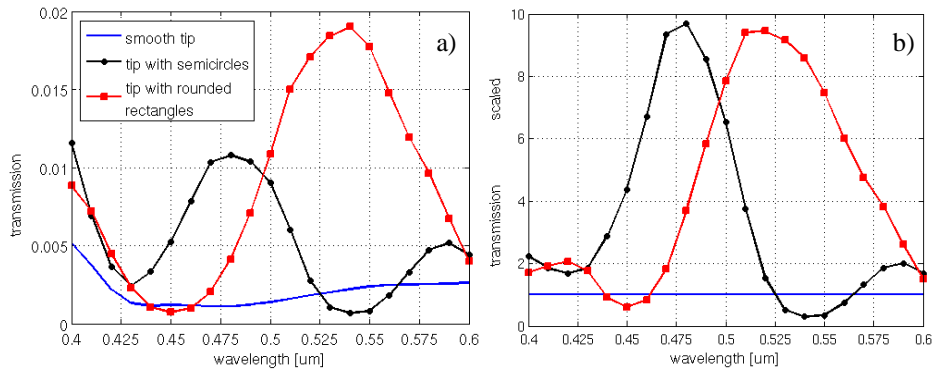


Fig. 2. Transmission of analyzed tips: a) absolute, and b) normalized to smooth tip transmission, calculated in the plane 10 nm outside the tip end.

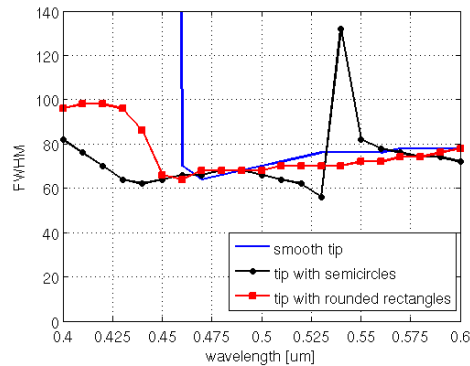


Fig. 3. FWHM of the beams emitted by the analyzed tips calculated in the plane 10 nm outside the tip end.

The FWHM of beams radiated by the tips defines the resolution achievable with SNOM when the tip-sample distance is kept constant. Any increase of output intensity can not worsen the FWHM in order for the energy throughput improvement to be of any use. In Fig. 3 we present the calculated FWHMs for simulated structures. For a classical tip the intensity of radiated

beams exceeds the tunneling-generated noise level only for wavelengths larger than 460 nm. For shorter wavelengths FWHM is undefined because of strong sidelobes. The widths of beams emitted from corrugated tips with both semicircular and rounded rectangular grooves are quite similar within the whole considered spectral range. A doubling of the FWHM observed at  $\lambda = 540$  nm for semicircular corrugations is not a numerical error and can be explained in terms of strong attenuation and reflection of the plasmon wave in that tip. It will be illustrated in subsequent figures.

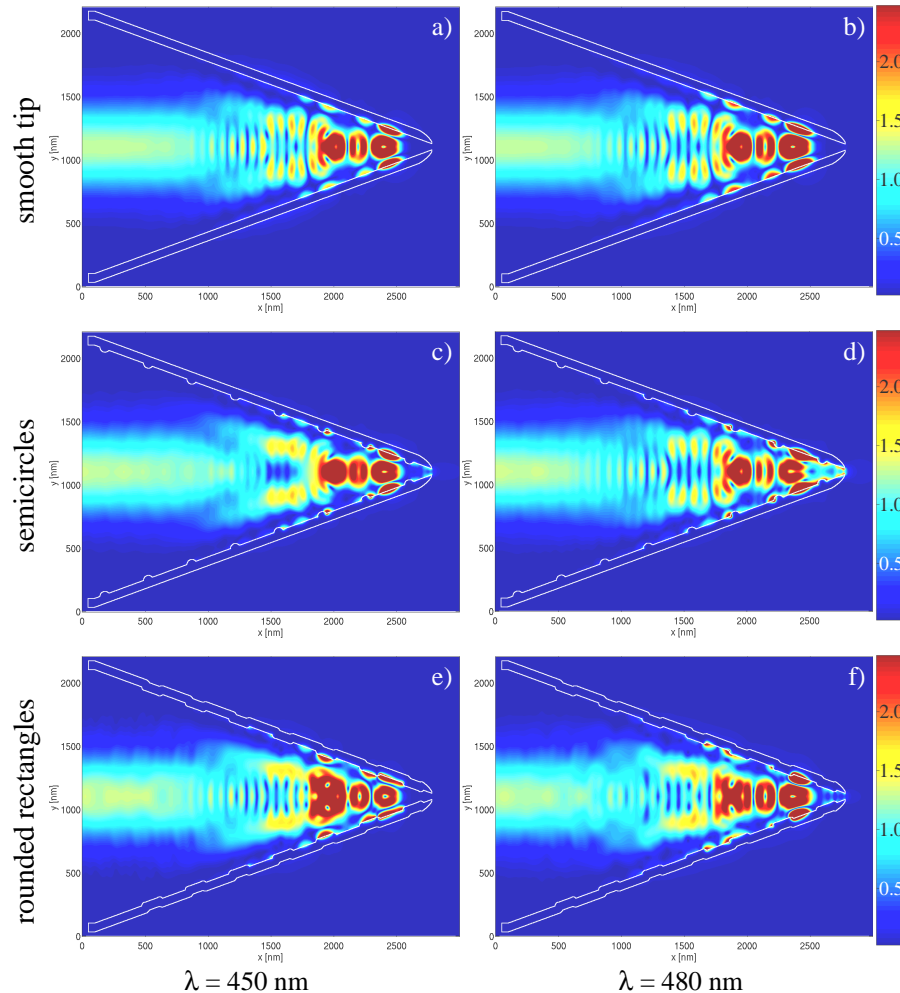


Fig. 4. Intensity distributions for wavelengths  $\lambda = 450$  nm (a, c, and e) and 480 nm (b, d, and f) in three considered types of tips averaged over the wave period. The white outline marks the boundary of the metal coating.

Intensity distributions shown in Figs. 4 and 5 illustrate how corrugations influence plasmon penetration of the tip end narrower than the cutoff diameter  $D$ . For probes with semicircular corrugations the highest intensity distribution in the outlet is observed for wavelength 480 nm (Fig 4(d)). For probes with rounded rectangular corrugations the highest intensity distribution in the outlet is observed for wavelength 540 nm (Fig 5(f)).

Figures 4 and 5 show distinct intensity distributions, averaged over the wave period, on the core-metal interface. In Figs 4 (a), (b) and 5 (a), (b) we observe a quasi-periodic intensity distribution and interpret it as a standing plasmon wave which results from interference of the incoming and reflected waves. A similar standing wave patterns are observed in all the

remaining subfigures except Fig. 5(d). This subfigure calculated for  $\lambda = 540$  nm and semicircular corrugations shows an especially high SPP intensity distribution, surprisingly connected with the lowest normalized transmission value (compare Fig. 2(b)). This specific case corresponds to an especially strong reflected plasmon wave. Thus reduction of the intensity of the reflected plasmon wave decides on high energy throughput.

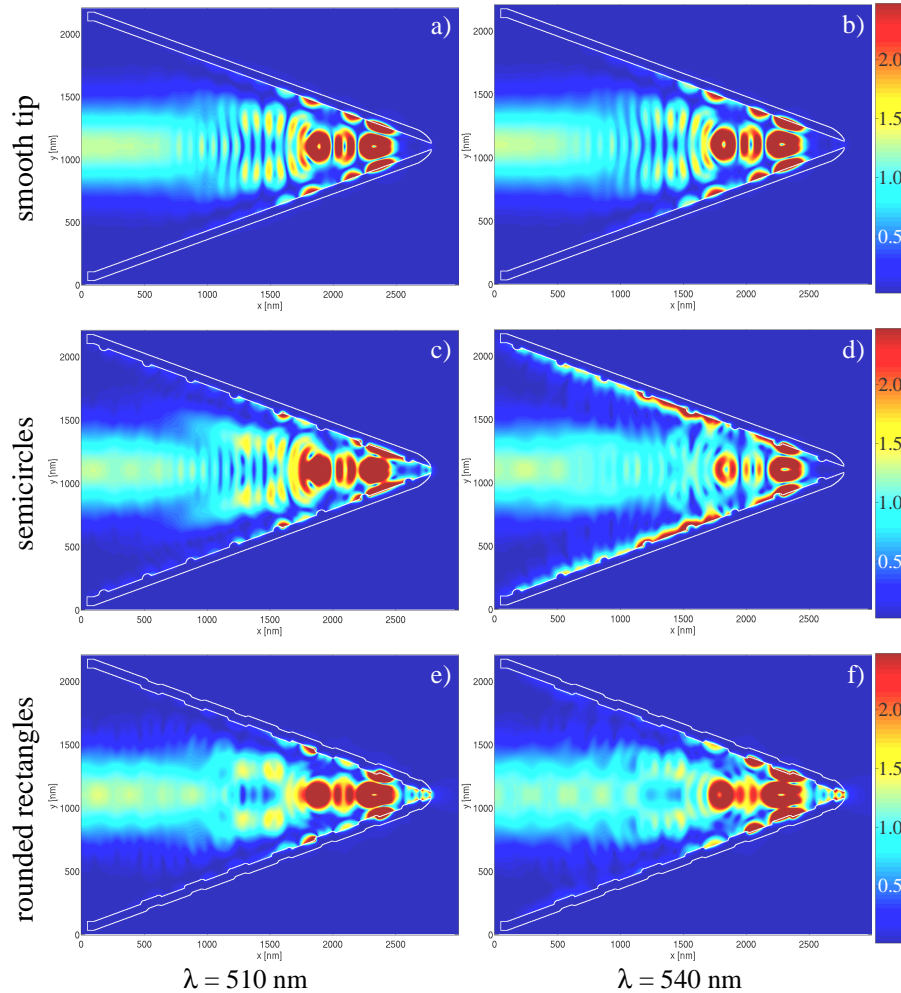


Fig. 5. Intensity distributions for wavelengths  $\lambda = 510$  nm (a, c, and e) and 540 nm (b, d, and f) in three considered types of tips averaged over the wave period. The white outline marks the boundary of the metal coating.

The rising slopes of metal ridges shown in blue and green in inlets in Fig. 6 and their positions with respect to the cutoff diameter location decide on efficient coupling of the incoming wave into corrugation localized plasmons. The intersection of colored lines with the black one correspond to the best light-to-plasmon coupling and highest energy throughput. The relative position of corrugations that enhance plasmon coupling and the cutoff diameter support the results shown in Fig. 2 (a) and (b). Namely, the maximum of transmission for the semicircular corrugation of Fig. 2(b) at  $\lambda = 480$  nm corresponds to the crossing of blue and black lines in Fig. 6. Analogously, the maximum of Fig. 2(b) at  $\lambda = 520$  nm agrees with the green-black crossing in Fig. 6.

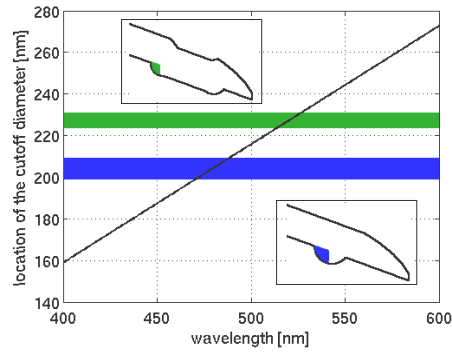


Fig. 6. The black line indicates the location of the cutoff diameter with respect to the tip end for different wavelengths. Locations of the rising slopes (colored blue and green in inlets) of the first corrugations from the tip end. The blue and green lines represents the position of semicircular and rectangular metal ridges with respect to the tip end.

Relative intensities calculated for probes with different corrugations at subsequent wavelengths are shown in Fig. 7. Here, the profiles are normalized with respect to the maximum point intensity of the smooth tip radiation independently within each subfigure.

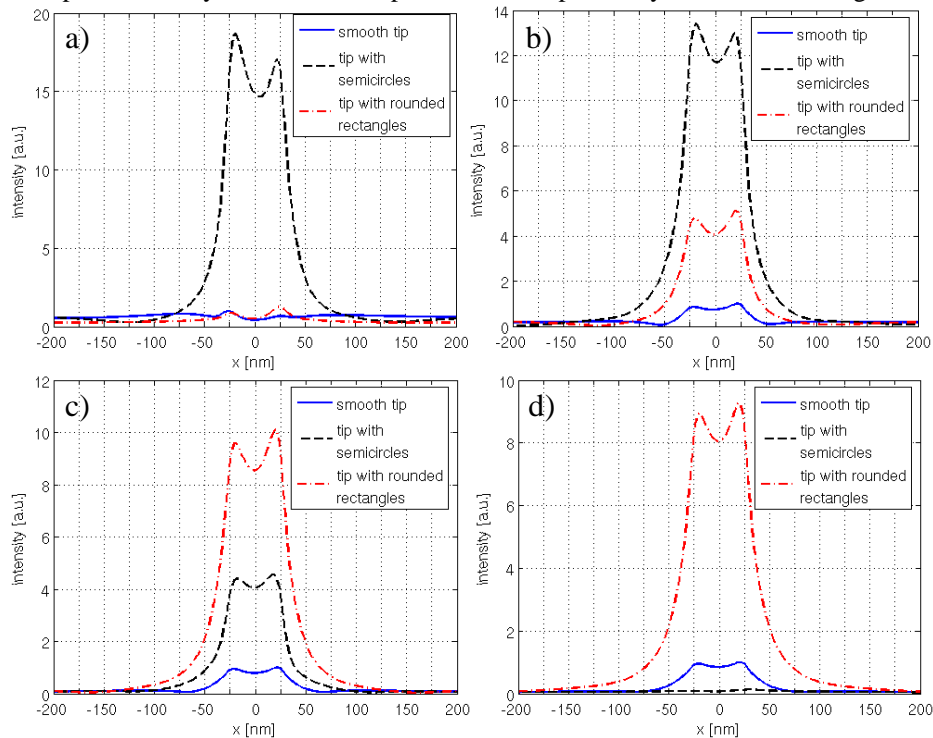


Fig. 7. Intensity profiles in the plane 10 nm outside the tip end calculated for three types of probes at wavelengths a) 450 nm, b) 480 nm, c) 510 nm and d) 540 nm. Within each subfigure plots are normalized with respect to the maximum point intensity of the smooth tip radiation.

For the above normalization, intensity values obtained from corrugated probes considerably exceed those from smooth ones, for 450 nm the gain reaches a factor of 18 for a probe with semicircular grooves. Plots in Fig. 7 are in seeming disagreement with plots of Fig. 2. For example, for semicircular corrugations and wavelength 450 nm in Fig. 2(b) the normalized transmission is about 4.2 while for 480 nm it is about 10. In Fig. 7 (a) and (b), in turn, the corresponding transmitted point intensity values are about 18 and 13, respectively. The

difference comes from the fact that for small wavelengths the plots of Fig. 2 calculated for the uncorrugated tip exhibit strong tunneling which increases the total energy radiated by the probe. This is illustrated by the continuous blue line in Fig. 7(a) in which tunneling gives a similar contribution as the aperture clearance radiation. Tunneling through the metal coating makes the output beams uncollimated. In agreement with our recent model of SNOM tip radiation [20] intensity plots presented in Fig. 7 clearly show maximums connected with rim radiation. However, in the FDTD simulations radiation from the aperture clearance gives a higher on-axis field intensity than predicted in our model.

#### **4. Conclusions**

When realized in practice, the idea of corrugated probes with high light throughput should increase spatial resolution of SNOMs and influence its use for precise measurements. This should make SNOM image interpretation more readable than nowadays. Small aperture SNOM probes should be useful as near-field point sources in point spread function and space variance measurements of flat superlenses [*e.g.* 36].

It is difficult to predict whether the proposed corrugation can be implemented in practice with reasonable accuracy. Etching of a fiber core does not leave its surface ideally flat as 0.5 nm pixel smoothness in our simulations. Metal sputtering, when made properly, can cover the core surface without undesired atom clusters. In spite of technological problems we expect that the corrugation should lead to better energy throughput than possible in the present generation of probes.

The corrugation parameters, such as their period, width and depth have to be optimized. Techniques of etching narrow and shallow grooves in silica fibers are investigated.

#### **Acknowledgements**

This research was sponsored by the Polish grant 37/COS/2006/03. We also acknowledge the support from the 6FP Network of Excellence Metamorphose and COST action P11.